Stationary Vortices behind a Flat Plate Normal to the Freestream in Incompressible Flow

PAUL L. COE*
Hofstra University, Hempstead, N. Y.

Introduction

CURRENT studies of the flow over a slender delta wing at high angles of attack and low subsonic speeds have led to a reconsideration of the problem of flow normal to a flat plate with two stationary vortices behind it.

The problem was first stated by Riabouchinski,[1] and later cited by Bateman[2] and Brown and Michael.[3] The discussion presented here is based on the fact that the results of Riabouchinski's analysis do not satisfy the condition of smooth outflow at the plate edges.

Statement of the Problem

Consider a flat plate of width $2a$ placed normal to a freestream with velocity U. Behind the plate there are two stationary vortices of strengths $-K$ and $+K$ at the points

$$Z_1 = X_0 + iY_0, \qquad Z_2 = X_0 - iY_0 \tag{1}$$

It is desired to find the position (X_0, Y_0) of these vortices, and their strength K, such that the following boundary conditions are satisfied. 1) The normal component of velocity vanishes on the plate surface. 2) The velocity remains finite at the plate edges (Smooth outflow condition). 3) The vortices remain stationary.

Analysis

By the introduction of the transformed plane,

$$\zeta = (Z^2 + a^2)^{1/2} \tag{2}$$

the complex potential, $W(Z) = \phi + i\psi$, can be written as follows:

$$W(Z) = -U(Z^2 + a^2)^{1/2} - iK \log\left[\frac{(Z^2 + a^2)^{1/2} - (Z_1^2 + a^2)^{1/2}}{(Z^2 + a^2)^{1/2} - (Z_2^2 + a^2)^{1/2}}\right] \tag{3}$$

Boundary condition 1), tangent flow, is automatically satisfied.

By differentiating Eq. (3) it is found that for dW/dZ to remain finite at the plate edges, $Z = \pm ia$, and hence satisfy boundary condition (ii), it is required that

$$U = iK[(Z_1^2 + a^2)^{-1/2} - (Z_2^2 + a^2)^{-1/2}] \tag{4}$$

Equation (4) is the smooth outflow condition which gives a relationship between U, K, and the position of the vortices. In order for the vortices to remain stationary, the complex velocity must be zero at points Z_1 and Z_2. A vortex will induce no velocity on itself, and hence its contribution must be subtracted from the complex potential before evaluating the complex velocity at point Z_1. Consequently boundary condition 3, stationary vortices is satisfied by requiring that

$$d/dZ\,[W(Z) + iK \log (Z - Z_1)]|_{Z=Z_1} = 0 \tag{5}$$

Performing the indicated differentiation, combining terms, and using L'Hopital's rule to evaluate the result at $Z = Z_1$ yields

$$UZ_1 - iKZ_1[(Z_1^2 + a^2)^{1/2} - (Z_2^2 + a^2)^{1/2}]^{-1} + iKa^2[2Z_1(Z_1^2 + a^2)^{1/2}]^{-1} = 0 \tag{6}$$

Separating equation (6) into its real and imaginary parts yields

$$2(X_0^2 - Y_0^2) + a^2 - [(X_0^2 - Y_0^2 + a^2)^2 + 4X_0^2Y_0^2]^{1/2} = 0 \tag{7}$$

and

$$K^2 = U^2(X_0^2 + Y_0^2)^4/8(X_0^2 - Y_0^2)^3 \tag{8}$$

Received June 5, 1972.
Index category: Jets, Wakes, and Viscid-Inviscid Flow Interactions.
* Instructor, Department of Engineering and Computer Sciences.

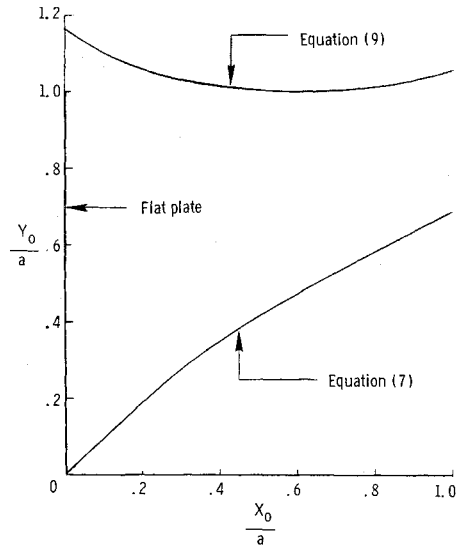

Fig. 1 Locus of stable vortex positions.

Repeating this analysis for the vortex at point Z_2 yields no additional information. Furthermore, it is found that by satisfying Eqs. (7) and (8), Eq. (4) is automatically satisfied.

Equation (7) yields a locus of points which will satisfy boundary conditions 1, 2, and 3 for vortices of strengths K given by equation (8). This locus is plotted in Fig. 1.

The locus of stationary vortices, and vortex strength K, as determined by Riabouchinski[1] are

$$Y_0(3)^{1/2} = -X_0 + 2(X_0^2 + a^2)^{1/2} \tag{9}$$

and

$$K^2(3)^{1/2} = 4U^2X_0Y_0 \tag{10}$$

When Eqs. (9) and (10) are substituted into the smooth outflow condition, Eq. (4), an identity should result, however, this is not the case. Riabouchinski's results are presented without detailed analysis and it is therefore difficult to find the error in his work. Equation (9) is plotted in Fig. 1 for comparison.

References

[1] Riabouchinski, D., "Sur Les Equations Du Mouvement A Deux Dimensions De Solides Dans Un Liquide Avec Tourbillons," *Comptes Rendus*, CLXXV, 1922, pp. 442–445.

[2] Bateman, H., *Partial Differential Equations of Mathematical Physics*, Dover, New York 1944, p. 254.

[3] Brown, C. and Michael, W., "On Slender Delta Wings with Leading Edge Separation," TN 3430, 1955, NACA.

Measurements of Particulate Pollutants in the Atmosphere

RAYMOND L. CHUAN*
Celesco Industries, A Division of The Susquehanna Corporation, Costa Mesa, Calif.

Introduction

MUCH of the pollutants in the atmosphere are in the form of solid and liquid particulates—or irregular conglomerates of molecules. While a complete description of the

Presented as Paper 71-1099 at the Joint Conference on Sensing of Environmental Pollutants, Palo Cito, Calif., November 8–10, 1971; submitted June 5, 1972; revision received August 4, 1972.
Index category: Aerospace Technology Utilization.
* Staff Assistant to President. Associate Fellow AIAA.

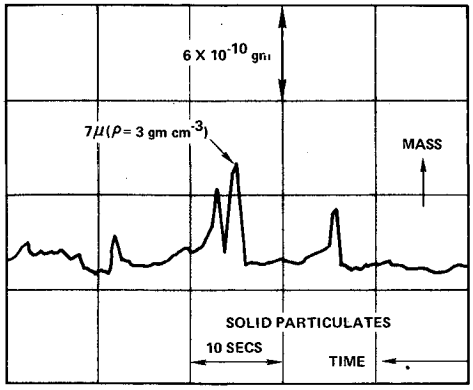

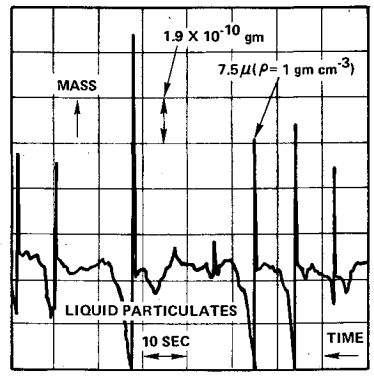

Fig. 1 Signatures of solid and liquid particulates.

polluted state of the atmosphere requires complete and detailed measurements of the chemical and physical composition of the atmosphere, a good gross gaging of pollution can be achieved by measuring the concentration of particulate matter. Clean air is defined by the California Air Resources Board as having a particulate mass concentration of less than 50 $\mu g/m^3$ (or 50 ppb by mass of the atmosphere). On a smog-alert day in Los Angeles the particulate mass concentration may be as high as 400 $\mu g/m^3$. A new type of instrument which evolved from efforts at measuring atmospheric density at orbital altitudes[1] is described here which measures directly, and in real time, the mass of particulate material suspended in the atmosphere. Typical examples of measurements are presented.

Description of the Instrument

The device is essentially an active impactor which is in the form of a small disc of piezo-electric crystal which forms part of a resonant circuit whose frequency is controlled by the mechanical resonant frequency of the crystal. In the present application the crystal, cut from quartz, operates in a shear mode whereby the opposite faces execute parallel displacements. In such a mode the frequency is affected by the mass on the crystal surface, such that for small oscillation amplitudes and small mass variations the resonant frequency is inversely proportional to mass:

$$\frac{\Delta f}{\Delta m} = -10^9 \text{ Hzg}^{-1} \text{ (for a nominal frequency of } 10^7 \text{ Hz)}$$

Since a frequency change of 10^{-2} is detectable by conventional electronic circuitry, it is seen that a mass detection of 10^{-11} g is possible with a 10^7 Hz crystal.

In practice the change in resonant frequency is detected by the change in beat frequency created by mixing the frequency of the sensing crystal with that of a reference crystal operating at a slightly higher frequency. In this arrangement an increase in mass on the sensing crystal results in an increase in the beat frequency. There is usually a slight temperature dependence of the frequency. However, by placing the reference crystal in the same thermal environment as that of the sensing crystal, temperature compensation is automatically achieved. To assure capture of particulate matter which impacts on the crystal, the latter is coated with about 10^{-4} cm of an adhesive material. Experience shows that particles from less than 10^{-4} cm diam to about 10^{-2} cm are retained by the coating with sufficient bond to render possible effective weighing of these particles with linear response. For convenience in data reduction the beat frequency is converted to an analog voltage which is, in turn, differentiated to yield mass change rate. In this way discrete impacts of particulates give rise to pulses in the differentiated signal, with the pulse height proportional to individual particulate mass as illustrated in Fig. 1. Calibrations[2] with a flow rate of 0.05 liter sec^{-1} drawn from a test chamber of 40 m^3 volume laden with a known quantity of particulates (micro-grit aluminum oxide with mass density of 3.89 g cm^{-3} and mean particle diameter of 3 μ) are shown in Fig. 2.

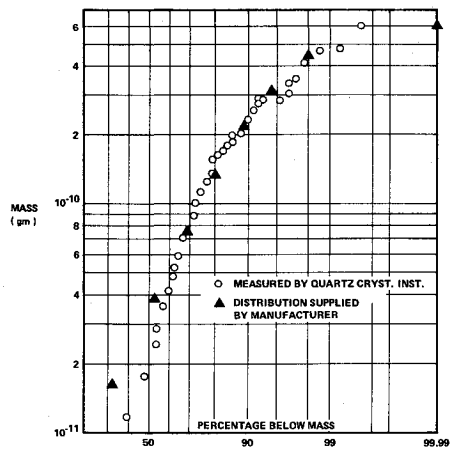

Fig. 2 Particulate mass distribution.

Examples of Particulate Measurements

Aerial measurement of atmospheric particulates

Since the instrument is quite compact and its output is in real time, aerial measurements can be easily made. The examples shown here were obtained with the instrument mounted in a light airplane, with an inlet probe attached to wing-strut. While continuous data was obtained over the entire flight, only representative data points are marked in Fig. 3. Figure 3 shows the results of a flight over a large part of the Los Angeles Basin. The minimum particulate mass concentration that could be resolved was about 2 μg^{-3}. It is seen from the data that the concentration at altitudes above 5000 ft was no higher than this minimum level. Part of the reason for this particular flight was to assess the effect of jet aircraft operation from airports in the area. Thus an approach was made to Los Angeles International Airport (LAX) from downwind. A high of 110 $\mu g\ m^{-3}$ was recorded 4 miles downwind to LAX at 1800 ft. Crosswind to the airport north towards Marina del Rey, the reading fell down to 20 $\mu g\ m^{-3}$. As the flight turned south across the takeoff path from LAX the concentration went up to 49 $\mu g\ m^{-3}$. Over the ocean at 6000 ft the concentration reached the limit of the instrument again.

Baghouse exhaust

The source was a large installation with a flow capacity of 500,000 cfm, filtering the fumes from four electric furnaces for processing scrap metal. Measurement of particles up to 5 μ diam using a dilution of 72:1 with clean dry bottled nitrogen was made of several compartments with exhaust temperature of 130°F. Comparable measurements had earlier been made by local pollution control officials using the conventional sampling train method with integrating times of up to 3 hr. Adjusting the latter results for particle size up to 5 μ (out of a total size range up to 74 μ) good agreement—2.5 mg m^{-3} by quartz crystal vs 2.3 mg m^{-3} by sampling train—was found.

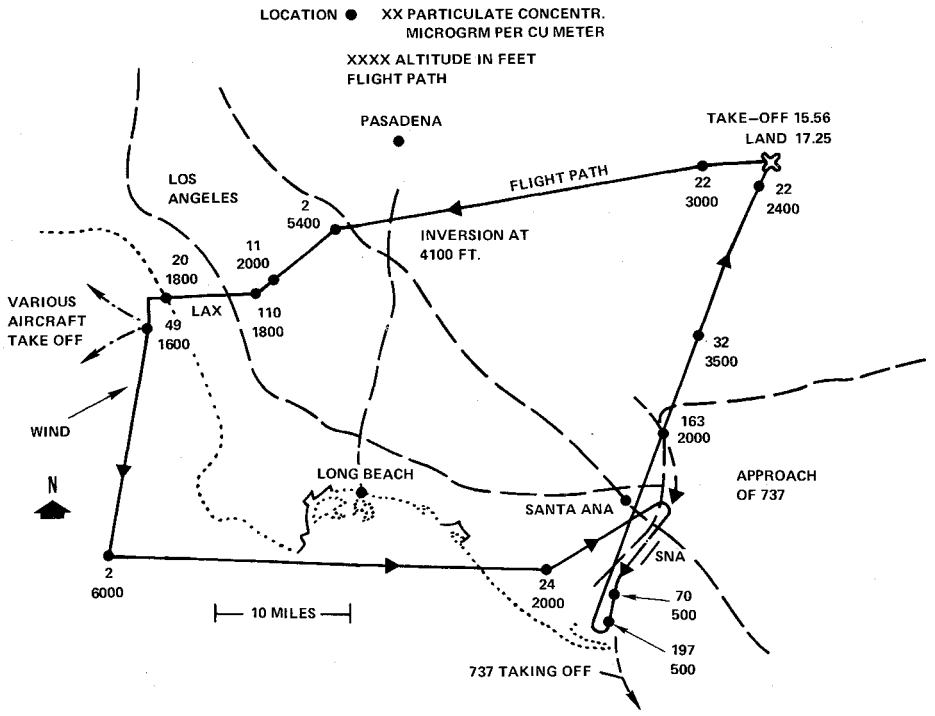

Fig. 3 Particulate concentration over Los Angeles basin.

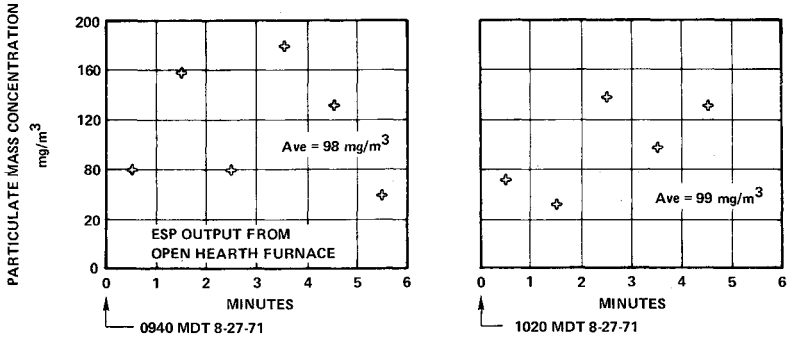

Fig. 4 In-stack particulate mass concentration.

Wet scrubber exhaust

The source was a rotary kiln for the production of light aggregates; and the control equipment was a sprayed-water scrubber. Some water droplets escaped into the atmosphere because of inadequate baffling, so that the conventional train method of measuring emissions took in air-borne as well as droplet-borne particulates. By using a diffuser to decelerate the flow into the sampling probe used with the quartz crystal instrument, it was possible to separate out the water droplets so that only air-borne particulates were measured. This accounts for the considerable difference between the quartz crystal measurement of 46 mg m^{-3} and the 188 mg m^{-3} value obtained by local enforcement officials using a sampling train.

Coal-fired electrical power plant

In-stack measurements of particulate mass concentration in the size range 0.1–2 μ were made in one of the units at the Arizona Public Service Co. generating complex at Farmington, N. Mex. The unit measured is equipped with an electrostatic precipitator and the measurements were made at the 250-ft level of the stack. Figure 4 shows particulate mass concentration data taken over 5-min intervals at two different times. Some of the fluctuation is believed to be real, while some of it is caused by unsteady flow in the sampling line due to oscillation of the isokinetic probe inserted into the stack. However, average concentration values are nearly identical for the two runs cited.

In order to assess the transport of the particulates from the stacks at Farmington, ambient air sampling was made from an aircraft along the path of the plume going generally downwind along the San Juan River. The results are shown in Fig. 5 for particulates in the size range 0.1–4 μ. The maximum concentration of 18 mg m^{-3} was measured as the aircraft passed directly over the stacks at 1000 ft above ground. The lowest concentration measured 12 miles down the plume was about 17 μg^{-3}, which was still more than three times the ambients concentration of about 5 $\mu g\ m^{-3}$ near Mesa Verde measured on the same flight at 10,000 ft above sea level. These aerial measurements were made in conjunction with an on-going program of the Los Alamos Scientific Lab. using a filter-type isokinetic sampler mounted on a B-57 aircraft. Analysis of the particulates collected on the

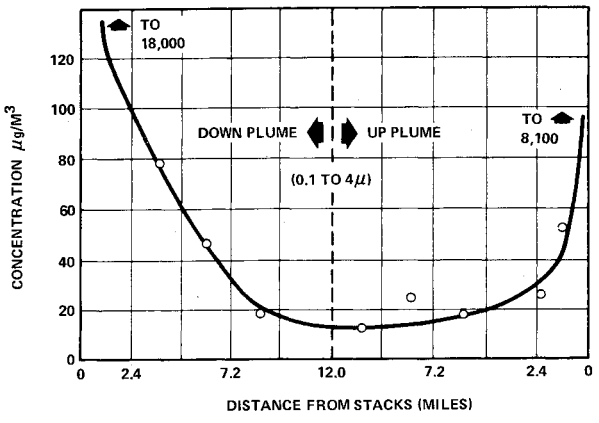

Fig. 5 Particulate mass concentration in plume.

quartz crystal from the quartz crystal instrument by Los Alamos confirmed the 4 μ cut-off. The average mass concentration of 30 $\mu g\ m^{-3}$ for the two passes (beginning and ending 1 mile from the stacks) also agrees with the Los Alamos measurement for particulates up to 4 μ.

Conclusion

By the various examples cited above, it has been demonstrated that a system derived from techniques acquired in the course of aerospace research and development can contribute effectively to the solution of problems relating to environmental issues. One can expect that the cross-fertilization among disciplines and the attendant broadening of perspectives should bring forth many advancements in measurement techniques for environmental pollution.

References

[1] Wainwright, J. B., "A Cryogenic Quartz Crystal Instrument for the Direct Measurement of Atmospheric Density," *Proceedings of the 3rd National Conference on Aerospace Meteorology*, American Meteorological Society, 1968, pp. 101–106.

[2] Chuan, R. L., "An Instrument for the Direct Measurement of Particulate Mass," *Journal of Aerosol Science*, Vol. 1, No. 2, May 1970, pp. 111–114.

Effect of Low Heat-Shield Ablation Rates on Flight Test Turbulent Base Pressure

BRUCE M. BULMER*
Sandia Laboratories, Albuquerque, N. Mex.

Nomenclature

A	= base area
K	= ratio of base pressure with mass addition to base pressure with no mass addition
M	= freestream Mach number
$\dot{m}$	= total heat-shield ablation (mass addition) rate
$\dot{m}/\rho VA$	= mass addition parameter
p_b	= base pressure
p_∞	= freestream pressure
R	= base radial coordinate
R_B	= base radius
R_N	= nose radius
R_N/R_B	= bluntness ratio
Re_L	= freestream Reynolds number based on axial length
V	= freestream velocity
θ_c	= cone half-angle
ρ	= freestream density

TURBULENT base pressure on full-scale re-entry vehicles (RV's) has been shown by Cassanto et al.[1,2] to depend upon the heat-shield ablation (mass addition) rate. These flight data, representing a wide range of ablation rates ($0.003 < \dot{m}/\rho VA < 0.05$), reveal that 1) mass addition increases the base pressure level, 2) mass addition creates radial base pressure gradients with the highest pressure occurring at the centerline, and 3) base pressure levels and gradients increase with increasing $\dot{m}/\rho VA$. This Note presents additional flight test data for two RV's having very low $\dot{m}/\rho VA$ (0.001 – 0.002) in turbulent flow and compares these data with other flight data and correlations.

The flight vehicles were relatively sharp ($R_N/R_B = 0.05$), slender ($\theta_c = 9°$) conical configurations having approximately flat bases. The re-entry trajectories were similar for both flights; during the period for which data are presented, the flow was hypersonic ($14 < M < 16.5$) and the angle of attack was less than 0.3°. The data were reduced by using calculated trajectories that included measured RV acceleration data and atmospheric conditions derived from radiosonde data.

Base pressure instrumentation consisted of thermal-conductivity type transducers[3] with high-sensitivity segmented output (0–50 torr range) designed to provide extremely accurate measurements to as low as 0.2% of full scale. The transducers, mounted near the centerline at $R/R_B = 0.1$, had no appreciable pressure time lag because of the very short pneumatic system (tube length/port diameter ratio of 12) and the negligible sensor volume.

The heat-shield ablation rates in turbulent flow are compared to those for other flight tests in Fig. 1. Ablation rates for the present flights were determined by use of a coupled solution between detailed ablating boundary layer and transient heat conduction calculations.[4] This solution technique has been verified by post-flight measurements of recovered heat-shield fragments from similar vehicles.

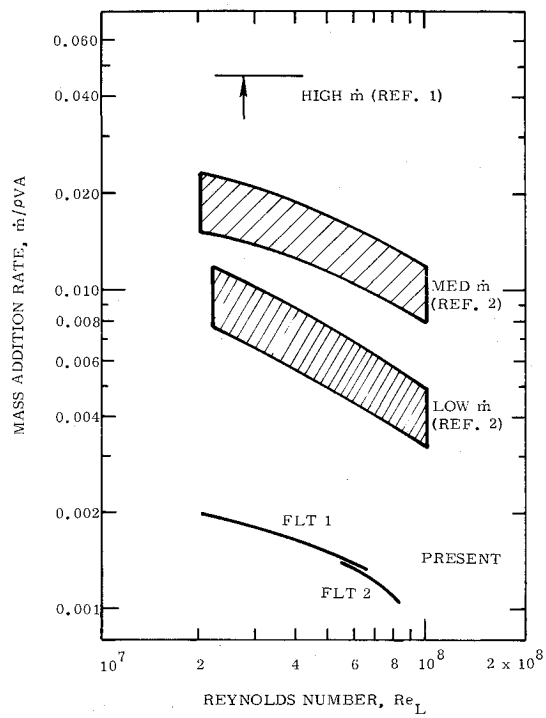

Fig. 1 Calculated heat-shield ablation rates in turbulent flow.

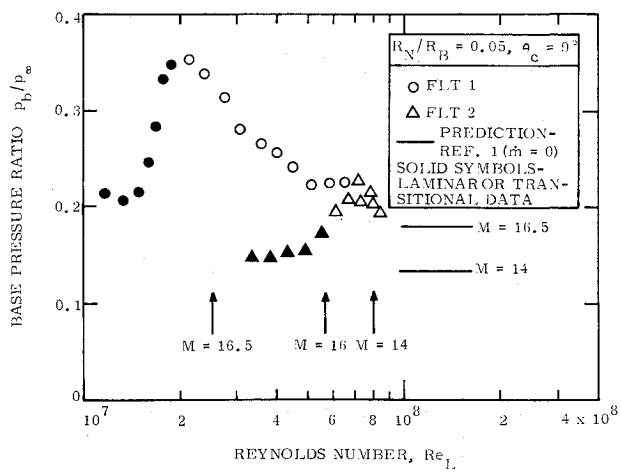

Fig. 2 Flight test base pressure data.

Received June 12, 1972. This work was supported by the U.S. Atomic Energy Commission.

Index categories: Re-Entry Vehicle Testing; Jets, Wakes, and Viscid-Inviscid Flow Interations.

* Member, Technical Staff, Re-Entry Vehicle Aerothermodynamics Division. Member AIAA.